Submitted to *Journal of Quantitative Spectroscopy and Radiative Transfer*, May 7, 2024

Mueller matrix symmetry for both reciprocal and nonreciprocal metamaterials

Chiyu Yang[1], Wenshan Cai[2], Zhuomin Zhang[1*]

[1]George W. Woodruff School of Mechanical Engineering, Georgia Institute of Technology, Atlanta, GA 30332, USA

[2]School of Electrical and Computer Engineering, Georgia Institute of Technology, Atlanta, GA 30332, USA

Mueller matrices relate the Stokes parameters of the incident and emerging light, providing useful information about the radiative properties and other characteristics of the medium. Determining all elements of the 4×4 Mueller matrix requires complete polarimetry, which is often challenging to perform. Partial polarimetry, on the other hand, uses simpler optical components in generating and/or analyzing states of polarization, thereby measuring only a subset of the Mueller matrix. However, it may determine the full Mueller matrix under specific symmetry conditions. The present study develops a symmetry classification scheme to categorize the Mueller matrix of materials. It is shown that the symmetry of the Mueller matrix is directly determined from the information of symmetries of the sample's optical properties. Numerical calculations of various measurement scenarios, structures, and materials (with or without Lorentz reciprocity) are carried out to validate the methodology. This study offers an insightful understanding of Mueller matrix symmetry and practical guidance for simplified ellipsometry measurements.

Keywords: Ellipsometry, metamaterial, Mueller matrix, partial polarimetry, radiative property.

[*] Corresponding Author: zhuomin.zhang@me.gatech.edu

Nomenclature

A	transformation matrix
a	period of grating, μm
$\vec{B}$	magnetic flux density, Tesla
$\vec{b}$	Weyl nodes separation vector, m^{-1}
C	constitutive matrix
C_n	n-fold rotational symmetry
c_0	speed of light in vacuum, m s^{-1}
$\vec{D}$	electric displacement vector, C m^{-2}
$\vec{E}$	electric field vector, V m^{-1}
$\vec{\vec{G}}$	dyadic Green's funtion
$\vec{H}$	magnetic field vector, A m^{-1}
$\vec{H}_0$	time-odd bias
h	height of grating, μm
I	3×3 identity matrix
I	inversion
i	$\sqrt{-1}$
J	Jones matrix
$\vec{J}$	electric source
k	isotropic amplitude absorption
L, L', C	complex parameters related to linear, 45° linear, and circular dichroism and birefringence, respectively
M	mueller matrix
$\vec{M}$	magnetization vector
M	element of the Mueller matrix
$\vec{r}$	position vector in a spherical coordinate
S	Stokes vector, V^2 m^{-2}
S_0, S_1, S_2, S_3	Stokes parameters, V^2 m^{-2}
s,p	TE- and TM-polarized
$\mathcal{T}$	adjoint transform
V	volume of the source current
w	width of grating, μm

x, y, z Cartesian coordinates

x', y' axes lying midway between the positive x- and positive y-axes, and negative x- and positive y-axes, respectively

Greek symbols

ε relative permittivity

$\vec{\vec{\varepsilon}}$ relative permittivity matrix

ε_0 vacuum permittivity, C V^{-1} m^{-1}

$\vec{\vec{\zeta}}$ electric-magnetic coupling strength matrix

η isotropic phase retardation

k isotropic absorption

Λ $\Lambda = \mathrm{sqrt}\,(L^2 + L'^2 + C^2)$

μ relative permeability

$\vec{\vec{\mu}}$ relative permeability matrix

μ_0 vacuum permeability, kg m s^{-2} A^{-2}

ξ reletive magnetoelectric coupling strength

$\vec{\vec{\xi}}$ magnetoelectric coupling strength matrix

σ mirror symmetry

ϕ, θ, r cylindrical coordinates

ω angular frequency, rad/s

Operators

T transpose

$\otimes$ Kronecker product

$*$ complex conjugate

1. Introduction

Wavelength-selective materials have enormous applications in energy and photonics systems, such as solar cells, solar absorbers, infrared emitters, and so on [1]. Micro/nanostructured metamaterials open the door of controlling electromagnetic waves over the phase, magnitude, and frequency [2]. Spectral, directional, and polarized-dependent infrared absorbers and emitters have been proposed based on anisotropic materials such as uniaxial hBN [3,4], biaxial MoO_3 [5] , and monoclinic Ga_2O_3 [6]; or constructed by patterned metasurfaces such as zig-zag nanorods [7], twisted gratings [8], and F-shape meta-atoms [9]. The radiative properties of micro/nanostructured metamaterials have been completely altered from their natural components. Therefore, it is of great significance to study and characterize the radiative properties of complex media.

Ellipsometry, a well-known noninvasive linear-optics technique, characterizes the physical and mechanical properties of materials using polarized light by measuring certain components of the Mueller matrix [10-13]. The Mueller matrix has a total of 4×4 elements that relate Stokes parameters of the incident and emerging (transmitted, reflected, or scattered) light after interaction with an object and carry information about the material properties. The information includes (i) dichroism, refers to the absorption difference between two polarized lights, (ii) birefringence, refers to the refractive indexes difference between two polarizations, and (iii) depolarization, denotes the reduction in the degree of polarization [10]. Determining all 16 Mueller matrix elements requires the use of a polarization state generator and a polarization state analyzer with 16 (or more) measurements, known as complete polarimetry. On the other hand, partial polarimetry uses a simpler generator and/or analyzer with a limitation to generate and/or analyze states of polarizations; thus, it measures a subset of the Mueller matrix [14]. For instance, circular dichroism spectrometer is a partial polarimeter optimized for measuring one of 16 elements of the Mueller matrix [15].

Partial polarimetry, however, could determine the full Mueller matrix under specific conditions. For instance, consider an isotropic medium with mirror symmetry to the plane of

incidence. In this scenario, the Jones matrix is diagonal, as the cross-polarization terms are zero, resulting in the Mueller matrix having zero off-diagonal blocks. Consequently, an ellipsometer equipped with linear generators and analyzers becomes sufficient to measure its complete Mueller matrix. Structures exhibiting symmetries can yield specific symmetric relations of Mueller matrices, thereby reducing the complexity of required polarimetric measurements. Arteaga et al. [14,16-18] have extensively discussed the symmetric relations of the Mueller matrix and explored the feasibility of using partial polarimetry to retrieve the complete Mueller matrix, focusing on the 9 and 12-element cases. Extensive studies on Mueller matrix symmetries can be found in Ref. [19-21]. Additionally, research on Mueller matrix has been carried out based on nonplanar diffraction gratings [22-25]. However, existing studies have primarily focused on reciprocal materials, which will lose validity when dealing with general bianisotropic media that can break the Lorentz reciprocity. Conversely, nonreciprocal metamaterials, such as multilayers and grating structures based on magneto-optical materials and magnetic Weyl semimetals, have shown unprecedented potential in polarization manipulation and energy transfer applications [26-28]. Therefore, understanding the symmetric relations of Mueller matrices without the constraint of reciprocity is imperative.

This study sheds light on the analysis of symmetric relations of Mueller matrix elements for specific measurement scenarios. By considering the symmetries of the structure and the measurement conditions, Mueller matrices are categorized into several classes, enabling the direct prediction of symmetric relations among their elements. The appropriateness of the theoretical framework is validated through numerical simulations involving both anisotropic and bianisotropic materials. Furthermore, the Mueller matrices of nonplanar structures, such as diffraction gratings, are examined to testify the applicability of the proposed methodology. The usage of symmetries classification scheme enables simpler combinations of polarimetry measurements for determining the complete Mueller matrix.

2. Background and theory

2.1. Nondepolarizing Mueller matrix

The Stokes vector $\mathbf{S} = (S_0, S_1, S_2, S_3)^T$, where T denotes the transpose operator, and the Poincaré sphere are commonly used in the polarimetric analysis of electromagnetic waves [11]. Each parameter represents measurable quantities with physical significance, corresponding to overall optical intensity, linearly polarized intensity, or circularly polarized intensity. For a medium interacting linearly with the incident electromagnetic wave and transforming the polarization state, it can be characterized by a 4×4 Mueller matrix **M**, consisting of 16 real elements denoted as [10,11]:

$$\begin{bmatrix} S_0 \\ S_1 \\ S_2 \\ S_3 \end{bmatrix}_{\text{out}} = \begin{bmatrix} M_{00} & M_{01} & M_{02} & M_{03} \\ M_{10} & M_{11} & M_{12} & M_{13} \\ M_{20} & M_{21} & M_{22} & M_{23} \\ M_{30} & M_{31} & M_{32} & M_{33} \end{bmatrix} \begin{bmatrix} S_0 \\ S_1 \\ S_2 \\ S_3 \end{bmatrix}_{\text{in}} \tag{1}$$

Here, the subscripts “in” and “out” refer to the incidence and emergence Stokes vectors, respectively. If **M** preserves the degree of polarization for any totally polarized incidence, it behaves as nondepolarizing, also known as the pure Mueller matrix, deterministic Mueller matrix, or Mueller-Jones Matrix [10]. The nondepolarizing Mueller matrix is derivable from a 2×2 Jones matrix **J** given by:

$$\mathbf{M} = \mathbf{A}(\mathbf{J} \otimes \mathbf{J})\mathbf{A}^{-1} \tag{2}$$

where $\otimes$ is the Kronecker product, and **A** is given by:

$$\mathbf{A} = \begin{bmatrix} 1 & 0 & 0 & 1 \\ 1 & 0 & 0 & -1 \\ 0 & 1 & 1 & 0 \\ 0 & i & -i & 0 \end{bmatrix} \tag{3}$$

and the Jones matrix takes the form:

$$\mathbf{J} = \begin{bmatrix} J_{pp} & J_{ps} \\ J_{sp} & J_{ss} \end{bmatrix} \tag{4}$$

The subscript p denotes a transverse magnetic (TM) wave and s denotes a transverse electric (TE) wave. The first and second indices of the subscript denote the incident and the emerging waves, respectively. Consequently, the nondepolarizing **M** has seven (7) degrees of freedom (DOF), corresponding to the eight (8) DOFs of the Jones matrix minus the absolute phase DOF [10,20]. Matrix **M** can be expressed in terms of Jones elements as:

$$\mathbf{M}=\begin{bmatrix} \frac{1}{2}\left(|J_{pp}|^2+|J_{ss}|^2+|J_{sp}|^2+|J_{ps}|^2\right) & \frac{1}{2}\left(|J_{pp}|^2-|J_{ss}|^2-|J_{sp}|^2+|J_{ps}|^2\right) & \mathrm{Re}\left(J_{pp}J_{sp}^*+J_{ss}^*J_{ps}\right) & \mathrm{Im}\left(J_{pp}J_{sp}^*+J_{ss}^*J_{ps}\right) \\ \frac{1}{2}\left(|J_{pp}|^2-|J_{ss}|^2+|J_{sp}|^2-|J_{ps}|^2\right) & \frac{1}{2}\left(|J_{pp}|^2+|J_{ss}|^2-|J_{sp}|^2-|J_{ps}|^2\right) & \mathrm{Re}\left(J_{pp}J_{sp}^*-J_{ss}^*J_{ps}\right) & \mathrm{Im}\left(J_{pp}J_{sp}^*-J_{ss}^*J_{ps}\right) \\ \mathrm{Re}\left(J_{pp}J_{sp}^*+J_{ss}^*J_{ps}\right) & \mathrm{Re}\left(J_{pp}J_{ps}^*-J_{ss}^*J_{sp}\right) & \mathrm{Re}\left(J_{pp}J_{ss}^*+J_{ps}^*J_{sp}\right) & \mathrm{Im}\left(J_{pp}J_{ss}^*-J_{ps}^*J_{sp}\right) \\ -\mathrm{Im}\left(J_{pp}J_{ps}^*+J_{ss}^*J_{sp}\right) & -\mathrm{Im}\left(J_{pp}J_{ps}^*-J_{ss}^*J_{sp}\right) & -\mathrm{Im}\left(J_{pp}J_{ss}^*+J_{ps}^*J_{sp}\right) & \mathrm{Re}\left(J_{pp}J_{ss}^*-J_{ps}^*J_{sp}\right) \end{bmatrix} \quad (5)$$

where * denotes the complex conjugate. This expression provides a straightforward indication of the symmetric relation between the Mueller matrix and the Jones elements. For instance, an isotropic medium with zero cross-polarization terms in the Jones matrix, i.e., $J_{ps} = J_{sp} = 0$, will result in zeroes off-diagonal blocks of the Mueller matrix. Furthermore, for light propagating in a continuous homogeneous medium, the Jones matrix can be expressed in terms of dichroisms and birefringence as [29]:

$$\mathbf{J}=e^{-i(\eta-ik)}\begin{bmatrix} \cos\frac{\Lambda}{2}-\frac{i\mathrm{L}}{2}\sin\frac{\Lambda}{2} & \frac{\mathrm{C}-i\mathrm{L}'}{2}\sin\frac{\Lambda}{2} \\ \frac{-\mathrm{C}-i\mathrm{L}'}{2}\sin\frac{\Lambda}{2} & \cos\frac{\Lambda}{2}+\frac{i\mathrm{L}}{2}\sin\frac{\Lambda}{2} \end{bmatrix} \quad (6)$$

where η and k are isotropic phase retardation and isotropic amplitude absorption, respectively. L, L′, and C are complex parameters related to linear dichroism and birefringence, 45° linear dichroism and birefringence, and circular dichroism and birefringence, respectively, and $\Lambda = \mathrm{sqrt}\,(\mathrm{L}^2 + \mathrm{L}'^2 + \mathrm{C}^2)$ (See Ref. [29] for more details). The diminishment of L, L′, or C will lead to specific patterns of the Jones elements, such as L = 0 leading to identical diagonal terms, L′ = 0 leading to opposite off-diagonal terms, and C = 0 leading to identical off-diagonal terms. Note that the Jones matrix provided by Eq. (6) is not equivalent to the transmission coefficients since the boundary condition has not been considered. However, it can be used to interpret the dichroism and birefringence behavior of boundary-induced transmission, and such interpretation is applicable to both transmission and

reflection modes. Therefore, for a nondepolarizing medium, the dichroism and birefringence parameters, the specific pattern of Jones elements, and the symmetric relation of the Mueller matrix, are related.

2.2. Symmetric relations of nondepolarizing Mueller matrix

The nondepolarizing Mueller matrix is said to exhibit symmetric relations if the off-diagonal elements possess the relations of the form $M_{ij} = \pm M_{ji}$. These relations are directly related to dichroism and birefringence parameters L, L′, and C. In other words, Mueller matrices with distinctive symmetric relations can be obtained by setting L, L′, or C of their corresponding Jones matrix to zero. Arteaga [16] provided a categorizing approach by assuming L′ = 0 and/or C = 0, resulting in four (4) distinct patterns of the Mueller matrix. Here, all three parameters are considered, and the relationships between dichroism and birefringence parameters, Jones matrix, and Mueller matrix are summarized in Table 1 [16,20]. Note that Jones and Mueller matrices belong to several classes when multiple parameters among L, L′, and C are zeros, such that the symmetric relation of the Mueller matrix is a superposition of each class. For instance, a Jones matrix with L = C = 0 falls into both classes II and III, resulting in the simultaneous satisfaction of $J_{sp} = J_{ps}$ and $J_{sp} = -J_{ps}$, leading to $J_{sp} = J_{ps} = 0$ for the Jones matrix and zero off-diagonal blocks for the Mueller matrix. If the matrices do not fall into any class, no symmetric relation can be established. The combination of these classes yields a total of eight (8) distinct patterns of the Mueller matrix.

Jones or Mueller matrices of any class possess a reduced number of independent Mueller matrix elements. Consequently, the full Mueller matrix can be obtained using partial polarimetry. For example, a partial polarimeter equipped with a full polarization state generator and a linear polarization state analyzer could determine up to 12 of the 16 elements of the Mueller matrix, which is adequate for determining the Mueller matrix falling into any of the classes. For matrices belonging to both classes II and III, a partial polarimeter with a linear polarization state generator and a linear

polarization state analyzer is sufficient. Further details regarding the ellipsometric measurement capabilities can be found in Ref. [30].

Table 1. Relationships between dichroism and birefringence, equivalence between Jones matrix elements, and symmetric relations of the Mueller matrix.

Class	I (L = 0)	II (L′ = 0)	III (C = 0)
J	$J_{ss} = J_{pp}$ (For transmission) $J_{ss} = -J_{pp}$ (For reflection)	$J_{sp} = -J_{ps}$ (For both transmission and reflection)	$J_{sp} = J_{ps}$ (For both transmission and reflection)
M	$\begin{bmatrix} M_{00} & M_{01} & M_{02} & M_{03} \\ -M_{01} & M_{11} & M_{12} & M_{13} \\ M_{02} & -M_{12} & M_{22} & M_{23} \\ M_{03} & -M_{13} & M_{23} & M_{33} \end{bmatrix}$ (For transmission) $\begin{bmatrix} M_{00} & M_{01} & M_{02} & M_{03} \\ -M_{01} & M_{11} & M_{12} & M_{13} \\ -M_{02} & M_{12} & M_{22} & M_{23} \\ -M_{03} & M_{13} & M_{23} & M_{33} \end{bmatrix}$ (For reflection)	$\begin{bmatrix} M_{00} & M_{01} & M_{02} & M_{03} \\ M_{01} & M_{11} & M_{12} & M_{13} \\ -M_{02} & -M_{12} & M_{22} & M_{23} \\ M_{03} & M_{13} & -M_{23} & M_{33} \end{bmatrix}$ (For both transmission and reflection)	$\begin{bmatrix} M_{00} & M_{01} & M_{02} & M_{03} \\ M_{01} & M_{11} & M_{12} & M_{13} \\ M_{02} & M_{12} & M_{22} & M_{23} \\ -M_{03} & -M_{13} & -M_{23} & M_{33} \end{bmatrix}$ (For both transmission and reflection)

2.3. Symmetry of the medium

Reciprocity plays an important role in determining the symmetric relations of the Mueller matrix based solely on the symmetry of the medium and the measurement scenario. The concept of reciprocity has a long history, and the most renowned electromagnetic reciprocity theorem was introduced by Lorentz in 1896 [31], stating the equivalence in the interchange of the source and the observer. Subsequently, in 1931, Onsager derived the general reciprocal relations based on statistical mechanics, which aligns with Lorentz reciprocity under time reversibility [32]. Considering electromagnetic radiation from fluctuating electric current, the electric field $\vec{E}$ at location $\vec{r}$ radiated by the electric source $\vec{J}$ at location $\vec{r}'$ is linearly related by the dyadic Greens function $\vec{\vec{G}}$ as [33]:

$$\vec{E}(\mathbf{r}) = \int_{V'} \vec{\vec{G}}(\vec{r},\vec{r}') \cdot \vec{J}(\vec{r}')dV' \tag{7}$$

where V' is the volume of the source current. For reciprocal participating media, the following relation can be obtained based on the Onsager relation:

$$\vec{\vec{G}}(\vec{r},\vec{r}') = \vec{\vec{G}}^T(\vec{r}',\vec{r}) \tag{8}$$

However, if there exists the external time-odd bias, reciprocity is broken and Eq. (8) is invalid. Examples include magneto-optical materials subjected to an external magnetic field or ferromagnetic materials after magnetization. On the other hand, Casimir introduced the Onsager-Casimir relations in 1945 to include nonreciprocal behaviors [34]. The dyadic Greens function derived from the Onsager-Casimir relations remains valid for both reciprocal and nonreciprocal media:

$$\vec{\vec{G}}(\vec{r},\vec{r}',\vec{H}_0) = \vec{\vec{G}}^T(\vec{r}',\vec{r},-\vec{H}_0) \tag{9}$$

where $\vec{H}_0$ denotes a signal parameter representing all time-odd bias fields of the system, and $-\vec{H}_0$ indicates the reversal of all fields. This equality applies to any linear, casual, time-reversible, and thermodynamic quasi-equilibrium system [33]. In the case when $\vec{H}_0 = 0$, Eq. (9) reduces to Eq. (8).

For a general linear metamaterial with time-odd bias $\vec{H}_0$, both electric and magnetic currents can be induced by incident electric and magnetic fields. The inhomogeneous constitutive relation can be described by the 6×6 matrix **C**, as given in [35,36], that relates the electric displacement vector $\vec{D}$ and magnetic flux density $\vec{B}$ with the electric field vector $\vec{E}$ and magnetic field vector $\vec{H}$ according to

$$\begin{bmatrix} \vec{D} \\ \vec{B} \end{bmatrix} = \mathbf{C}\left(\omega,\vec{r},\vec{H}_0\right)\begin{bmatrix} \vec{E} \\ \vec{H} \end{bmatrix} = \begin{bmatrix} \varepsilon_0\vec{\vec{\varepsilon}}\left(\omega,\mathbf{r}\right) & c_0^{-1}\vec{\vec{\xi}}\left(\omega,\mathbf{r}\right) \\ c_0^{-1}\vec{\vec{\zeta}}\left(\omega,\mathbf{r}\right) & \mu_0\vec{\vec{\mu}}\left(\omega,\mathbf{r}\right) \end{bmatrix}\begin{bmatrix} \vec{E} \\ \vec{H} \end{bmatrix} \tag{10}$$

Here, $\vec{\vec{\varepsilon}}$, $\vec{\vec{\mu}}$, $\vec{\vec{\xi}}$, and $\vec{\vec{\zeta}}$ are 3×3 matrices representing dimensionless electric permittivity, magnetic permeability, and the cross-coupling between the electric and magnetic fields, respectively, ε_0, μ_0, and c_0 denotes the vacuum permittivity, permeability, and speed of light, respectively, and ω is the angular frequency. The medium with **C** encompasses different types of materials ranging from isotropic to

bianisotropic. For instance, **C** represents: (i) isotropic material when $\ddot{\varepsilon}$ and $\ddot{\mu}$ are reduced to scalar and $\ddot{\xi} = \ddot{\zeta} = 0$, (ii) bi-isotropic material when all four 3×3 matrices $\ddot{\varepsilon}$, $\ddot{\mu}$, $\ddot{\xi}$, and $\ddot{\zeta}$ reduce to scalars, (iii) anisotropic material if $\ddot{\xi} = \ddot{\zeta} = 0$, or (iv) bianisotropic material with the full 6×6 matrix. An example of a bianisotropic material is an artificial composite metamaterial made of split-ring resonators [37,38], where such material has an effective 6×6 constitutive matrix despite each composite material being isotropic. Reversing the time-odd bias fields alters the constitutive relation as [36]:

$$\mathcal{T}\mathbf{C}(\omega,\vec{r},\vec{H}_0) = \mathbf{C}(\omega,\vec{r},-\vec{H}_0) = \begin{bmatrix} \varepsilon_0\ddot{\varepsilon}^T(\omega,\mathbf{r}) & -c_0^{-1}\ddot{\xi}^T(\omega,\mathbf{r}) \\ -c_0^{-1}\ddot{\zeta}^T(\omega,\mathbf{r}) & \mu_0\ddot{\mu}^T(\omega,\mathbf{r}) \end{bmatrix} \tag{11}$$

where $\mathcal{T}$ denotes the adjoint transform [36] that reverses the time-odd bias fields, and the system with reversed time-odd bias fields is referred to the adjoint system. The adjoint transform is well-defined and physically realizable. For instance, $\mathcal{T}$ applied to nonreciprocal magneto-optical materials is equivalent to reversing the external magnetic field, while $\mathcal{T}$ applied to reciprocal materials will not alter the material properties (see Ref. [36] for more details), thus being $\mathcal{T}$-invariant. With the help of $\mathcal{T}$, one can rewrite Eq. (9) to include the constitutive relations as

$$\ddot{G}(\vec{r},\vec{r}',\mathbf{C}) = \ddot{G}^T(\vec{r}',\vec{r},\mathcal{T}\mathbf{C}) \tag{12}$$

The relation between two Jones elements can be derived with the help of Eq. (12). Consider a planar structure with a constitutive matrix **C** as shown in Figure 1a. The system is subject to a *s*-polarized incidence at a zenith angle θ in the *x*-*z* plane through port 1, and a *p*-polarized specular reflection through port 2. The reflection Fresnel coefficient is written as $r_{1s2p}(\mathbf{C})$. According to Eq. (12), its adjoint system with an opposite propagation direction (as shown in Figure 1b) must yield the same Fresnel reflection coefficient as

$$r_{1s2p}(\mathbf{C}) = -r_{2p1s}(\mathcal{T}\mathbf{C}) \tag{13}$$

Note that there is a negative sign on the right-hand side of the equation because of the reversed direction of incidence, which requires altering the positive direction of either p or s when defining the Fresnel coefficient.

Therefore, if the planar layer **C** is invariant to the combination of adjoint transform and a 180° rotation transform with respect to z axis, the planar layer **C** is said to possess compound symmetry $\mathcal{T}C_2(z)$ and its reflection coefficients have $r_{sp} = -r_{ps}$. Such that the symmetric relation of the corresponding Mueller matrix can be categorized into class II. The symmetries of a given sample **C** may include both geometric symmetries such as mirror symmetry σ and n-fold rotational symmetry C_n, and compound symmetries such as $\mathcal{T}\sigma$ and $\mathcal{T}C_n$, which represent the invariance of the system by combining the adjoint transform $\mathcal{T}$ with geometric transform [39,40]. Therefore, a comprehensive search is needed to relate the symmetries to the reflection coefficients.

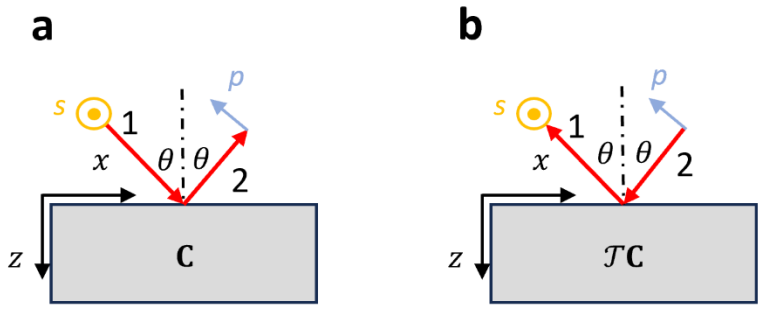

Figure 1. The original system and the adjoint transformed system. The original system has constitutive tensor **C** with s-polarized incidence at angle θ in the x-z plane through port 1 and a p-polarized specular reflection through port 2; the adjoint system has the constitutive tensor $\mathcal{T}$**C** with reversed propagation waves from port 2 to port 1.

To illustrate the symmetries searching process, Figure 2 is used as an example to demonstrate the required transformation and the corresponding symmetry for class III ($J_{sp} = J_{ps}$) at normal reflection. The initial step is to look for transformations capable of converting the wave vector configuration from s-polarized incidence p-polarized reflectance to p-polarized incidence s-polarized

reflectance. There will be two unique paths through geometric transformation noted as path A and B, and two unique paths through compound transformation noted as path C and D. If the sample is invariant under these transformations, the sample is said to possess the corresponding symmetries and the reflection coefficients have $r_{sp} = r_{ps}$. Therefore, these symmetries lead to the Mueller matrix exhibiting specific patterns as categorized in class III. Here, paths A and B correspond to the medium exhibiting 4-fold rotational symmetry $C_4(z)$ with respect to the z-axis, while paths C and D indicate compound mirror symmetries $\mathcal{T}\sigma(yz)$ and $\mathcal{T}\sigma(xz)$,

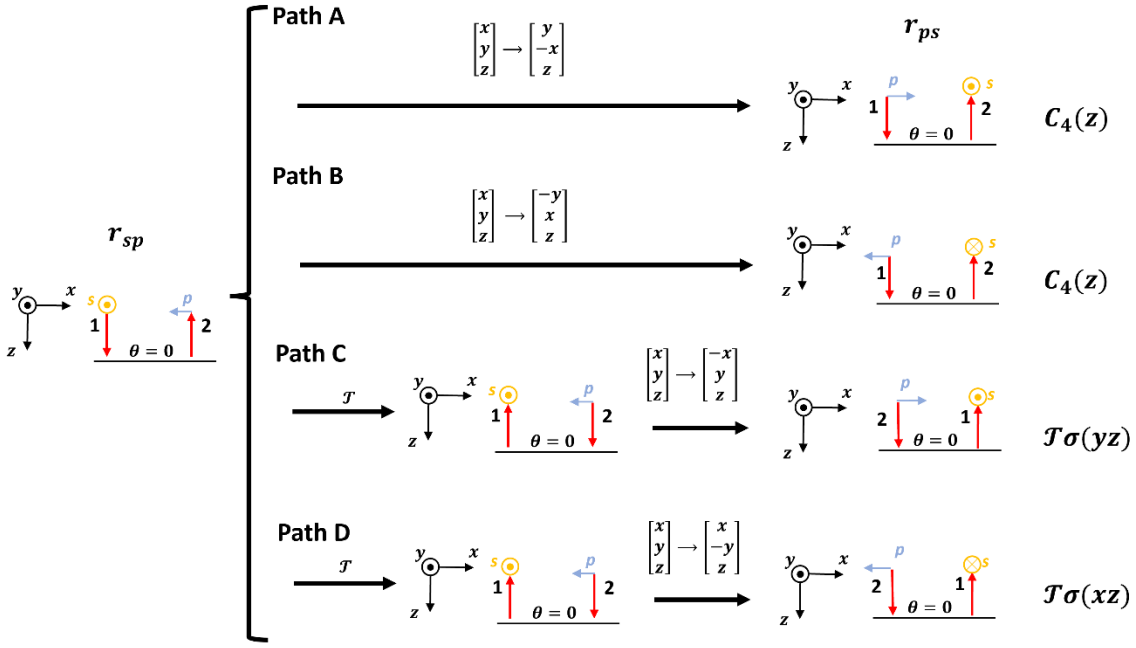

Figure 2. Symmetries searching process for class III ($J_{sp} = J_{ps}$) at normal reflection. A total of two geometric transform paths (A and B) plus two compound transform paths (C and D) were found to convert the wave system of r_{sp} to r_{ps}. If the sample is invariant under the transform paths, signifying class III, the sample is said to possess the corresponding symmetry.

respectively. A unique instance not attainable through these transformations but still leading to class III is when the sample consistently has $J_{sp} = 0$ and $J_{ps} = 0$. It means the relation of $J_{sp} = J_{ps}$ is always satisfied. This condition is achieved by a medium exhibiting mirror symmetry with respect to the plane of incidence, $\sigma(yz)$, yielding zero off-diagonal Jones elements. Consequently, four symmetries, $C_4(z)$, $\mathcal{T}\sigma(yz)$, $\mathcal{T}\sigma(xz)$, and $\sigma(yz)$, can lead to the class III symmetric relations of Mueller matrix. A

similar procedure can be applied to identify the symmetries of classes I or II for various measurement scenarios including reflection or transmission measurement at normal or oblique incidence. Notably, for oblique incidence, no symmetry can yield $J_{ss} = J_{pp}$, resulting in an empty class I. The symmetries for each class under various measurement scenario are summarized in Table 2. Here, x' denotes the axis lying midway between the positive x- and positive y-axes, y' represents the axis lying midway between the negative x- and positive y-axes, and I denotes inversion. Note that an object with high symmetry inherently includes lower symmetries; for example, $C_4(z)$ includes $C_2(z)$, and $\mathcal{T}C_6(z)$ includes both $C_3(z)$ and $\mathcal{T}C_2(z)$. The symmetries tabulated in this classification scheme represent the lowest symmetries that will result in a particular class.

Table 2. Symmetries for each measurement scenario.

Class	Jones matrix	Symmetries			
		Oblique incidence		Normal incidence	
		Transmission	Reflection	Transmission	Reflection
I	$J_{ss} = J_{pp}$ (For transmission) $J_{ss} = -J_{pp}$ (For reflection)	N/A	N/A	$\sigma(x'z)$ $\sigma(y'z)$ $C_4(z)$ $\mathcal{T}\sigma(xy)\sigma(x'z)$ $\mathcal{T}\sigma(xy)\sigma(y'z)$ $\mathcal{T}\sigma(xy)C_4(z)$	$\sigma(x'z)$ $\sigma(y'z)$ $C_4(z)$ $\mathcal{T}\sigma(x'z)$ $\mathcal{T}\sigma(y'z)$ $\mathcal{T}C_4(z)$
II	$J_{sp} = -J_{ps}$ (For both transmission and reflection)	$\mathcal{T}C_2(y)$ $\sigma(xz)$	$\mathcal{T}C_2(z)$ $\sigma(xz)$	$C_4(z)$ $\mathcal{T}C_2(x)$ $\mathcal{T}C_2(y)$ $\sigma(xz)$	$\sigma(x'z)$ $\sigma(y'z)$ $\mathcal{T}C_2(z)$ $\mathcal{T}$ $\sigma(xz)$
III	$J_{sp} = J_{ps}$ (For both transmission and reflection)	$\mathcal{T}I$ $\sigma(xz)$	$\mathcal{T}\sigma(yz)$ $\sigma(xz)$	$\sigma(x'z)$ $\sigma(y'z)$ $\mathcal{T}\sigma(xy)$ $\mathcal{T}C_2(x)$ $\sigma(xz)$	$C_4(z)$ $\mathcal{T}\sigma(yz)$ $\mathcal{T}\sigma(xz)$ $\sigma(xz)$

Unlike the nondepolarizing Mueller matrix, which preserves the degree of polarization, the depolarizing Mueller matrix transforms some or all totally polarized incident states into partially polarized or unpolarized emerging states. This transformation is caused by scattering, spatial inhomogeneity, or the inherent spatial, spectral, or temporal averaging nature of measurement devices

[10,20]. For instance, a film sample has no interference effect due to its thickness is greater than the coherence length. Detailed formulations for calculating the radiative properties of thick films using the ray-tracking method without the interference effect can be found in Ref. [1].

Depolarizing Mueller matrix has a total of 16 degrees of freedom due to the depolarizing contributions. It cannot be converted into a single Jones matrix. However, the depolarizing Mueller matrix can be linearly decomposed into up to four nondepolarizing Mueller matrices [10]. Therefore, if a depolarizing and inhomogeneous medium satisfies the symmetries tabulated in Table 2, one can still categorize its Mueller matrix into specific classes in Table 1, since the matrix is the sum of all nondepolarizing Mueller matrix components.

For measurement scenario based on a diffraction medium where the emergence angle is not equal to the incidence angle, the relations outlined in Table 2 will not hold, as the symmetries are determined under the assumption of specular reflection and transmission. However, if the wave interaction remains specular, the symmetry classification scheme remains applicable. An example is the zeroth-order diffraction of a grating structure.

3. Numerical verification

Two sets of structures are used to validate the methodology. The first set includes planar slab and multilayer structures with specular reflection and/or transmission. The second set consists of grating structures with multiple propagation diffractions.

3.1. Planar structures

The 4×4 transfer matrix method, originally put forward by Teitler and Henvis [41,42], has been extensively used to compute the Fresnel coefficients of anisotropic slabs and multilayer

structures. This method can be extended to calculate bianisotropic multilayer structures with a full constitutive tensor [43]. Five types of metamaterials, including biaxial, gyroelectric, gyromagnetic, magnetoelectric, and multilayer structures, are utilized to demonstrate the appropriateness of the methodology. Symmetries can be either determined via performing transformations to the structure schematics, or by applying an equivalent mathematical transform on the constitutive tensors. With the help of symmetry analysis, Mueller matrices of each example are categorized into classes. In the following examples, a consistent wavelength of 5 μm, layer thickness of 1 μm, and an incidence angle of $\theta = 45°$ for oblique incidence are chosen for all slabs and multilayer structures.

The first type of structure is planar slab made of biaxial crystal, characterized by three principal axes corresponding to the crystalline directions [100], [001], and [010]. Biaxial materials are reciprocal, thus being $\mathcal{T}$-invariant. Calculations are carried out based on the dielectric function of the α-phase MoO_3 [44]. Figures 3a – 3c depict three scenarios of reflectance measurement for the biaxial slab with different principal axis orientations. The constitutive tensors and the resulting Mueller matrices are provided on the right side of the schematics. In the first scenario depicted in Figures 3a with oblique incidence, the [100] principal axis of the medium is aligned with the z-axis direction, while the rest are arbitrarily oriented. Predicted from the methodology, the structure corresponds to class II due to the $\mathcal{T}C_2(z)$ symmetry. This is confirmed by the resultant Mueller matrix having $J_{sp} = -J_{ps}$. In the second scenario as shown in Figure 3b, the [001] principal axis is aligned with the x-axis direction. $\mathcal{T}\sigma(yz)$ symmetry is identified, and the corresponding class is III according to both prediction and calculation. Figure 3c illustrates a scenario with normal light incidence and all principal axes arbitrarily oriented. The symmetry obtained is $\mathcal{T}$, and the corresponding class is II.

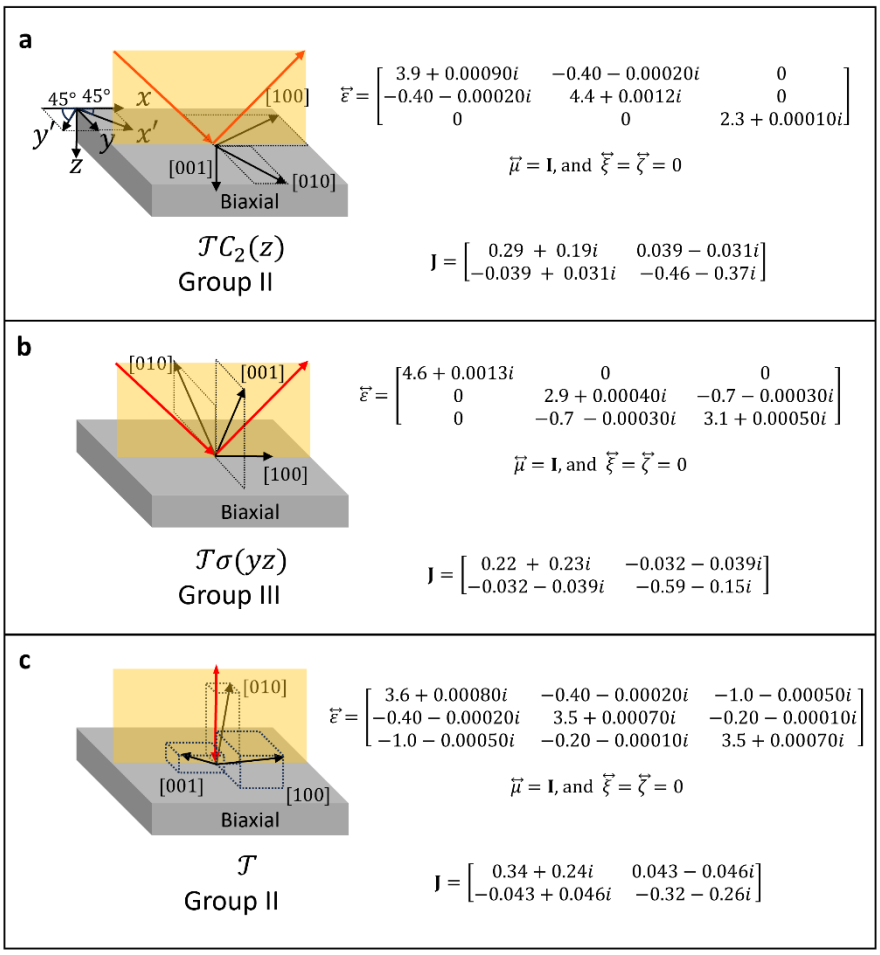

Figure 3. Scenarios of reflectance measurement for the biaxial slab with different principal axis orientations. Biaxial crystal at $\theta = 45°$ incidence with (a) [100] principal axis in z-axis direction while the rest are arbitrarily oriented and (b) [001] principal axis in x-axis direction, (c) and at normal incidence with all principal optics axes arbitrarily oriented.

The second set of scenarios as depicted in Figures 4a-4c are reflectance measurements for gyroelectric slabs. These slabs are characterized by a tensorial $\vec{\vec{\varepsilon}}$ with opposite off-diagonal elements, a scalar $\ddot{\mu}$, and $\vec{\vec{\xi}} = \vec{\vec{\zeta}} = 0$ [43,45]. Examples include magneto-optical materials [46,47], magnetic Weyl semimetals [48], and topological insulators [49]. The off-diagonal terms are induced by the external magnetic field $\vec{B}$ for magneto-optical materials or due to Weyl node separation $\vec{b}$ in momentum space for magnetic Weyl semimetals. These vectors are pseudovectors and comply with pseudovector rules when transformed by reflection or inversion [50]. For simplicity, they are uniformly denoted as $\vec{B}$ in the schematics. It is assumed that the material is isotropic with diagonal

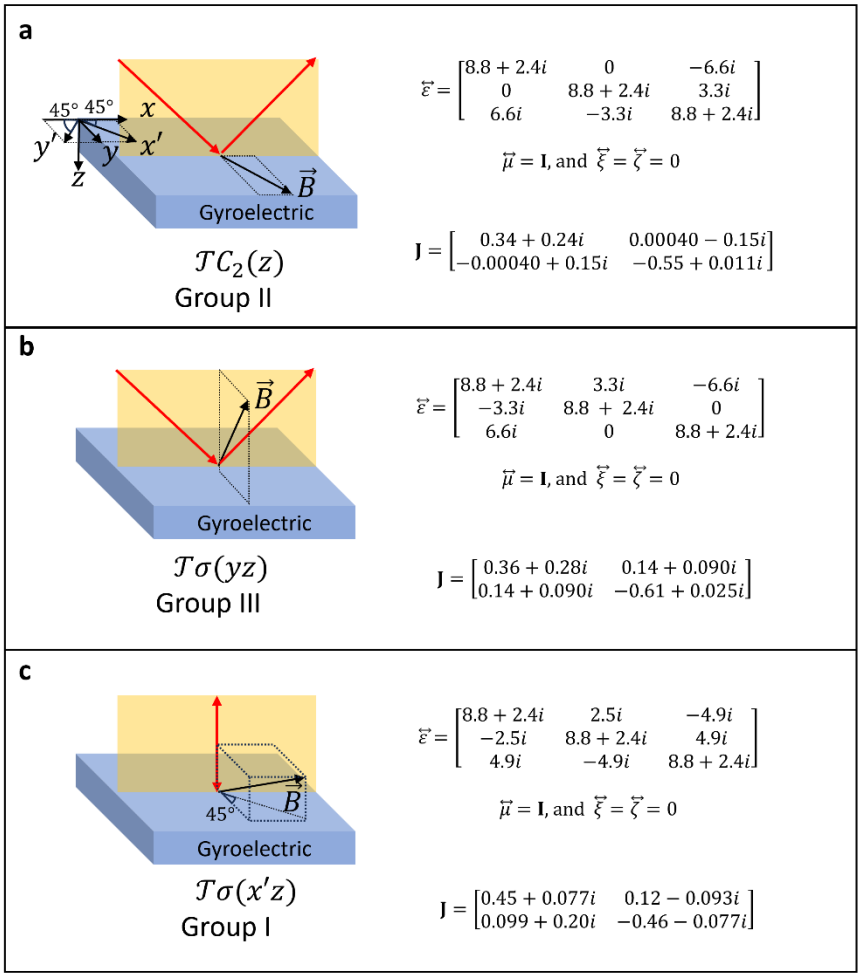

Figure 4. Scenarios of reflectance measurement for gyroelectric slabs with different magnetic field orientations. At $\theta = 45°$ incidence with magnetic field $\vec{B}$ arbitrarily oriented (a) in x-y plane and (b) in y-z plane, and (c) at normal incidence with $\vec{B}$ lies in x'-z plane.

permittivity, i.e., $\varepsilon_x = \varepsilon_y = \varepsilon_z$. Calculations are based on the dielectric function of magnetic Weyl semimetals [27]. Gyroelectric materials are nonreciprocal, and $\mathcal{T}$ will result in the reversal of vector $\vec{B}$. In the scenario depicted in Figure 4a, the gyroelectric slab with the magnetic field arbitrarily oriented in the x-y plane is illuminated by light at an oblique incidence angle. Through a combination of the adjoint transform and a 2-fold rotation transform with respect to the z-axis, an invariant structure is obtained, resulting in the $\mathcal{T}C_2(z)$ symmetry of the structure. The corresponding Mueller matrix affiliates with class II. Figure 4b depicts a scenario with the magnetic field arbitrarily oriented in the y-z plane. Here, the symmetry obtained is $\mathcal{T}\sigma(yz)$ and the resultant Mueller matrix is within class III. Figure 4c illustrates normal light incidence on the structure with the magnetic field $\vec{B}$

arbitrarily oriented in the x'-z plane. In this case, the structure shows $\mathcal{T}\sigma(x'z)$ symmetry, leading to class I for the corresponding Mueller matrix.

The example depicted in Figure 5 is for the transmitted Mueller matrix of a gyromagnetic slab under oblique light incidence. Typically, gyromagnetic materials, such as ferromagnets and ferrites [43,45], are characterized by a scalar $\vec{\vec{\varepsilon}}$, a tensorial $\vec{\vec{\mu}}$ with opposite off-diagonal elements, and $\vec{\vec{\xi}} = \vec{\vec{\zeta}} = 0$. Calculations are based on a constant constitutive tensor as provided by Ref. [43]. When magnetized to saturation by an external DC magnetic field, gyromagnetic materials acquire a tensorial magnetic permeability with the magnetization pseudovector denoted by $\vec{M}$, which conforms to the same rules as the magnetic field $\vec{B}$ follows. In the schematic, the magnetization vector $\vec{M}$ lies in the x-z plane. Therefore, the $\mathcal{T}C_2(y)$ symmetry within the structure results in class II for the corresponding Mueller matrix.

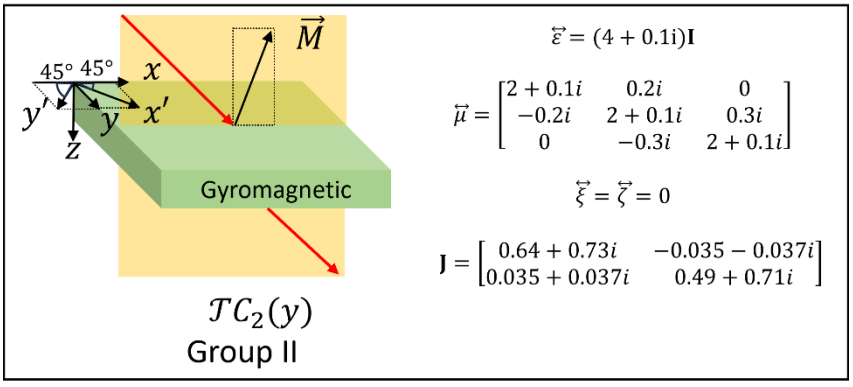

Figure 5. Scenarios of transmittance measurement for a gyroelectric slab at an incidence angle of $\theta = 45°$ and the magnetization $\vec{M}$ oriented in the x-z plane.

In magnetoelectric materials, such as the natural materials like Cr_2O_3 and $TbPO_4$ [51], the magnetic field induces electric dipoles and electric field induces magnetic dipoles. Additionally, the magnetoelectric effect has been observed in nano/microstructures such as split-ring resonators [52,53]. Figures 6a and 6b illustrate scenarios of reflectance measurements of split-ring resonator-based metasurfaces with oblique incidence. The pattern of the metasurface is in the subwavelength range,

allowing the material to be considered homogeneous with a constitutive tensor approximated by effective medium theory [37,38]. In Figure 6a, the unit cell of split ring resonator-based structure is depicted with the ring split facing toward the negative *y*-axis. Here, magnetic field in the *z*-direction will induce electric dipoles in the *x*-direction due to the asymmetry of the split-ring structure. Likewise, electric field in the *x*-direction generates unbalanced currents, leading to magnetic dipoles in the *z*-direction. Consequently, the effective electric-magnetic cross-coupling

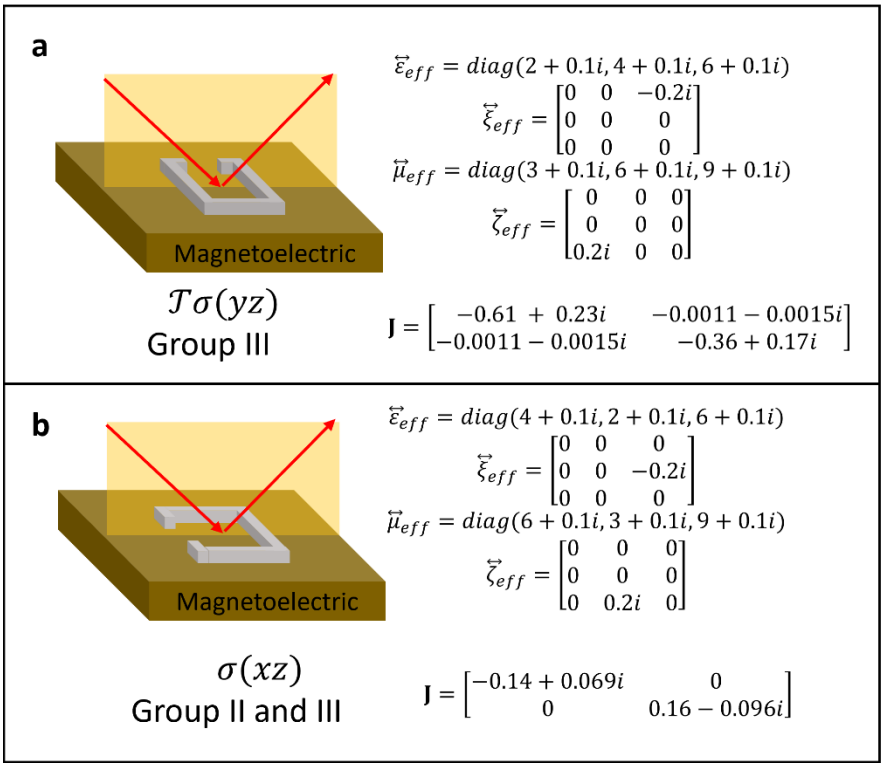

Figure 6. Scenarios of reflectance measurement for effective magnetoelectric materials based on split ring resonator with the ring split facing toward (a) negative y-axis and (b) negative *x*-axis direction.

tensors have nonzero elements $\vec{\xi}_{13} = -i\xi$ and $\vec{\zeta}_{31} = i\xi$. The permittivity $\vec{\varepsilon}$ and permeability $\vec{\mu}$ are diagonal. Such split-ring-based metasurface is reciprocal and $\mathcal{T}$-invariant. A representative constant constitutive tensor is used for calculation. With $\mathcal{T}\sigma(yz)$ symmetry, the Mueller matrix of the structure belongs to class III. In contrast, the ring split of structure shown in Figure 6b is facing toward the negative *x*-axis direction, leading to nonzero electric-magnetic cross-coupling terms $\vec{\xi}_{23} = -i\xi$ and

$\vec{\vec{\zeta}}_{32} = i\xi$. Since this structure exhibits mirror symmetry $\sigma(xz)$, the resultant Mueller matrix is within both classes II and III simultaneously. This results in zero off-diagonal blocks in the Mueller matrix.

The last scenario as depicted in Figure 7 involves transmittance measurement of a multilayer structure with oblique light incidence. Here, a gyroelectric layer with a magnetic field oriented in the negative x-axis is placed on the top of an isotropic slab. The calculation is based on magnetic Weyl semimetal for gyroelectric material and glass for isotropic material. Although each single slab holds $\mathcal{T}C_2(y)$ symmetry, their combination shows no symmetry, and the resultant Mueller matrix does not attach to any of the classes.

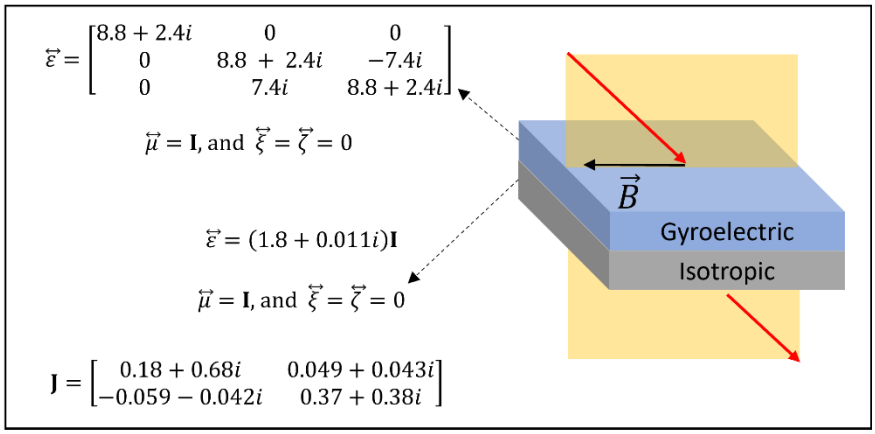

Figure 7. Oblique incidence on a multilayer structure without exhibiting any symmetry. The top layer is a gyroelectric slab with $\vec{B}$ oriented in negative x-axis, and the bottom layer is isotropic.

The calculated Mueller matrices for planar structures as described above validate the prediction from symmetry classification scheme. Moreover, other scenarios as given in Ref. [16] also find consistency with the proposed methodology.

3.2. Grating structures

In this section, examples of nonplanar structures are studied with both reciprocal and nonreciprocal diffraction gratings are considered. The first example is an aluminum grating subjected

to conical light incidence as shown in Figure 8. This grating has a period $a = 4$ μm, width $w = 3.6$ μm, and height $h = 1.2$ μm. At the chosen wavelength $\lambda = 4$ μm, the dielectric function $\varepsilon = -1405+521i$. The zenith angle and azimuthal angle of incidence are set to $\theta = 80°$ and $\phi = 45°$, respectively. Given that a is comparable to λ, multiple propagation diffraction orders are presented.

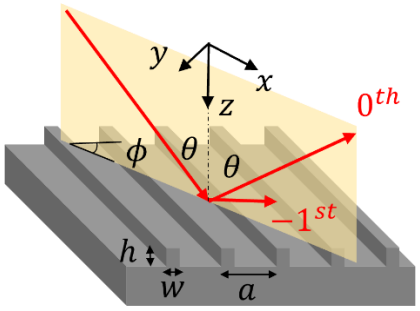

Figure 8. A diffraction grating with a conical incidence with two propagating diffraction orders. The aluminum grating with relative permittivity $\varepsilon = -1405+521i$ and geometrical parameters $a = 1$ μm, $w = 0.54$ μm, and $h = 0.39$ μm, is placed on the substrate of the same material. Operation wavelength is selected at $\lambda = 4$ μm with a zenith angle of incidence $\theta = 80°$ and tilted plane of incidence at $\phi = 45°$. Propagating diffracted waves are marked by solid arrows with -1^{st} and 0^{th} represent the diffraction orders.

Rigorous coupled-wave analysis (RCWA) [3] is employed for the calculations. The analysis reveals that the -1^{st} and 0^{th} orders are propagating, with their reflection Jones matrix given as:

$$\mathbf{J}^{-1st} = \begin{bmatrix} -0.21+0.004i & 0.04-0.009i \\ 0.32-0.006i & -0.06+0.007i \end{bmatrix} \tag{14}$$

For the -1^{st} diffraction order, and

$$\mathbf{J}^{0th} = \begin{bmatrix} -0.35-0.320i & 0.24+0.076i \\ -0.24-0.076i & -0.95-0.006i \end{bmatrix} \tag{15}$$

For the 0^{th} diffraction order. Note that the elements of $\mathbf{J}^{0th}$ satisfy relation $J_{sp} = -J_{ps}$, which corresponds to symmetry class II. This is because the specular reflectance condition is met for the 0^{th} diffraction order and the structure exhibits $\mathcal{T}C_2(z)$ symmetry. However, for $\mathbf{J}^{-1st}$, no relation is found among Jones elements since the -1^{st} diffraction order violates the specular reflection condition.

The second set of nonplanar structures as depicted in Figure 9a and 9b consist of two nonreciprocal diffraction gratings based on magnetic Weyl semimetals. Both gratings have a period $a = 7$ μm, width $w = 3.5$ μm, and height $h = 1.2$ μm. For the calculations, an operational wavelength $\lambda = 9$ μm, incidence zenith angle $\theta = 45°$, and incidence azimuthal angle $\phi = 45°$ are selected. Though multiple propagation diffraction orders exist, only the 0^{th} order reflection is discussed. These two gratings exhibit different symmetries. The permittivity tensor of the first grating and its substrate is given by

$$\vec{\vec{\varepsilon}} = \begin{bmatrix} -1.41+0.476i & 0 & -9.41i \\ 0 & -1.4+0.476i & 9.41i \\ 9.41i & -9.41i & -1.4+0.476i \end{bmatrix} \tag{16}$$

It describes a Weyl node separation $\vec{b} = 2\ \mathrm{nm}^{-1}$ aligns with the grating stripe direction [54]. The grating exhibits $\mathcal{T}C_2(z)$ symmetry and the calculated Mueller matrix should be within class II. The Jones matrix becomes

$$\mathbf{J}^{0\mathrm{th}} = \begin{bmatrix} 0.31+0.488i & 0.38-0.331i \\ -0.38+0.331i & -0.56-0.410i \end{bmatrix} \tag{17}$$

has $J_{sp} = -J_{ps}$ that aligns with the prediction. In contrast, the latter structure has $\vec{b} = 2\ \mathrm{nm}^{-1}$ along the negative z-axis direction, with the permittivity tensor:

$$\vec{\vec{\varepsilon}} = \begin{bmatrix} -1.41+0.476i & -13.3i & 0 \\ 13.3i & -1.4+0.476i & 0 \\ 0 & 0 & -1.4+0.476i \end{bmatrix} \tag{18}$$

Unlike the former scenario, rotation with respect to the z-axis has no effect on the pseudovector $\vec{b}$ while $\mathcal{T}$ will reverse its direction. Consequently, $\mathcal{T}C_2(z)$ symmetry is broken, and no symmetry can be identified for this structure. The corresponding Mueller matrix, calculated using RCWA, is given as:

$$\mathbf{J}^{0\mathrm{th}} = \begin{bmatrix} 0.40+0.360i & -0.10+0.110i \\ -0.29+0.095i & -0.73-0.320i \end{bmatrix} \tag{19}$$

which does not belong to any of the symmetry classes. Note that according to the incomprehensive classification criteria as given in Refs. [17,18], the structure has rotational symmetry, and the Mueller matrix should fall within class II. In this study, the classification scheme provides accurate prediction with the help of symmetries. Thus, the proposed methodology demonstrates its applicability in analyzing nonplanar diffraction structures.

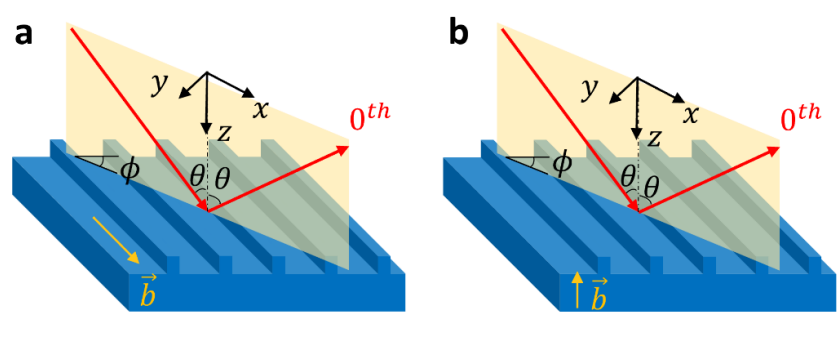

Figure 9. Scenarios of reflectance measurement for nonreciprocal diffraction gratings based on magnetic Weyl semimetals with (a) Weyl node separation $\vec{b}$ along the grating stripe direction, and (b) along the grating stripe direction, and along the direction of negative z-axis. Both gratings have a period a = 7 μm, width w = 3.5 μm, and height h = 1.2 μm. Operation wavelength is selected at λ = 9 μm with a zenith angle of incidence θ = 45° and tilted plane of incidence at ϕ = 45°.

Conclusion

This study sheds light on the relationships between the Mueller matrix and the symmetries of structures, proposing a symmetry classification scheme to predict the pattern of Mueller matrix, that is applicable to both reciprocal and nonreciprocal materials. The symmetries of measured sample and the measurement conditions will result in specific symmetric relations among the Mueller matrix elements. This allows the reduction of independent elements of Mueller matrix. Numerical simulations of various structures including biaxial, gyroelectric, gyromagnetic, and magnetoelectric materials, are carried out to validate the appropriateness of the methodology. Multilayer structures and nonplanar diffraction gratings, with or without reciprocity, are analyzed to illustrate the capability

and limitation. This work offers an analytical framework for understanding the symmetric relations of Mueller matrices, with practical implications for easier ellipsometry measurements.

CRediT authorship contribution statement

Chiyu Yang: Conceptualization, Data curation, Formal analysis, Investigation, Methodology, Validation, Visualization, Writing – original draft, Writing – review & editing. **Wenshan Cai**: Supervision, Writing – review & editing. **Zhuomin Zhang**: Conceptualization, Funding acquisition, Investigation, Resources, Supervision, Visualization, Writing – review & editing.

Acknowledgements

This work was supported by the U.S. National Science Foundation (CBET-2029892 for C.Y. and DMR-2004749 for W.C.) and the U.S. Department of Energy (DE-SC0018369 for Z.M.Z.).

Conflicts of interest

The authors declare no conflicts of interest.

Data availability

Data are available upon request.

References

[1] Zhang ZM. Nano/Microscale Heat Transfer. 2nd ed: Springer; 2020.

[2] Cai W, Shalaev VM. Optical Metamaterials: Springer; 2010.

[3] Zhao B, Zhang ZM. Perfect mid-infrared absorption by hybrid phonon-plasmon polaritons in hBN/metal-grating anisotropic structures. Int J Heat Mass Transf. 2017;106:1025-34.

[4] Wu X, Fu C, Zhang ZM. Chiral response of a twisted bilayer of hexagonal boron nitride. Opt Commun. 2019;452:124-9.

[5] Larciprete MC, Dereshgi SA, Centini M, Aydin K. Tuning and hybridization of surface phonon polaritons in α-MoO_3 based metamaterials. Opt Express. 2022;30:12788-96.

[6] Centini M, Yang C, Larciprete MC, Antezza M, Zhang ZM. Optimization of highly circularly polarized thermal radiation in α-MoO_3/β-Ga_2O_3 twisted layers. arXiv:2310.138012023. Submitted to J Quant Spectrosc Radiat Transf.

[7] Nguyen A, Hugonin J-P, Coutrot A-L, Garcia-Caurel E, Vest B, Greffet J-J. Large circular dichroism in the emission from an incandescent metasurface. Optica. 2023;10:232-8.

[8] Yang C, Cai W, Zhang ZM. Tailoring full-Stokes thermal emission from twisted-gratings structures. Nanophotonics 2024;13:803-11.

[9] Wang X, Sentz T, Bharadwaj S, Ray SK, Wang Y, Jiao D, et al. Observation of nonvanishing optical helicity in thermal radiation from symmetry-broken metasurfaces. Sci Adv. 2023;9:eade4203.

[10] Gil JJ, Ossikovski R. Polarized light and the Mueller matrix approach. 2nd ed: CRC press; 2022.

[11] Goldstein DH. Polarized Light. 3rd ed: CRC press; 2011.

[12] Francoeur M, Venkata PG, Mengüç MP. Sensitivity analysis for characterization of gold nanoparticles and agglomerates via surface plasmon scattering patterns. J Quant Spectrosc Radiat Transf. 2007;106:44-55.

[13] Klusek C, Manickavasagam S, Mengüç MP. Compendium of scattering matrix element profiles for soot agglomerates. J Quant Spectrosc Radiat Transf. 2003;79-80:839-59.

[14] Arteaga O, Kahr B. Mueller matrix polarimetry of bianisotropic materials. J Opt Soc Am B. 2019;36:F72-F83.

[15] Chabay I, Holzwarth G. Infrared Circular Dichroism and Linear Dichroism Spectrophotometer. Appl Opt. 1975;14:454-9.

[16] Arteaga O. Useful Mueller matrix symmetries for ellipsometry. Thin Solid Films. 2014;571:584-8.

[17] Arteaga O, Ossikovski R. Complete Mueller matrix from a partial polarimetry experiment: the 12-element case. J Opt Soc Am A. 2019;36:416-27.

[18] Ossikovski R, Arteaga O. Complete Mueller matrix from a partial polarimetry experiment: the nine-element case. J Opt Soc Am A. 2019;36:403-15.

[19] van de Hulst HC. Light scattering by small particles: Courier Corporation; 1981.

[20] Savenkov SN. Jones and Mueller matrices: structure, symmetry relations and information content. In: Kokhanovsky AA, editor. Light Scattering Reviews 4: Single Light Scattering and Radiative Transfer: Springer; 2009. p. 71-119.

[21] Arteaga O, Maoz BM, Nichols S, Markovich G, Kahr B. Complete polarimetry on the asymmetric transmission through subwavelength hole arrays. Opt Express. 2014;22:13719-32.

[22] Novikova T, Bulkin P, Popov V, Haj Ibrahim B, De Martino A. Mueller polarimetry as a tool for detecting asymmetry in diffraction grating profiles. J Vac Sci Technol B. 2011;29:051804

[23] Heinrich A, Bischoff J, Meiner K, Richter U, Mikolajick T, Dirnstorfer I. Interpretation of azimuthal angle dependence of periodic gratings in Mueller matrix spectroscopic ellipsometry. J Opt Soc Am A. 2015;32:604-10.

[24] Chen X, Gu H, Jiang H, Zhang C, Liu S. Robust overlay metrology with differential Mueller matrix calculus. Opt Express. 2017;25:8491-510.

[25] Wang M, Löhle A, Gompf B, Dressel M, Berrier A. Physical interpretation of Mueller matrix spectra: a versatile method applied to gold gratings. Opt Express. 2017;25:6983-96.

[26] Yang C, Cai W, Zhang ZM. Polarimetric analysis of thermal emission from both reciprocal and nonreciprocal materials using fluctuation electrodynamics. Phys Rev B. 2022;106:245407.

[27] Yang C, Zhao B, Cai W, Zhang ZM. Mid-infrared broadband circular polarizer based on Weyl semimetals. Opt Express. 2022;30:3035-46.

[28] Zhang Z, Zhu L. Nonreciprocal Thermal Photonics for Energy Conversion and Radiative Heat Transfer. Phys Rev Appl. 2022;18:027001.

[29] Arteaga O, Canillas A. Analytic inversion of the Mueller-Jones polarization matrices for homogeneous media. Opt Lett. 2010;35:559-61.

[30] Hauge PS. Recent developments in instrumentation in ellipsometry. Surf Sci. 1980;96:108-40.

[31] Lorentz HA. The theorem of Poynting concerning the energy in the electromagnetic field and two general propositions concerning the propagation of light. Versl Kon Akad Wet Amst. 1896;4:176-87.

[32] Onsager L. Reciprocal Relations in Irreversible Processes. I. Physical Review. 1931;37:405-26.

[33] Asadchy VS, Mirmoosa MS, Diaz-Rubio A, Fan S, Tretyakov SA. Tutorial on electromagnetic nonreciprocity and its origins. Proc IEEE. 2020;108:1684-727.

[34] Casimir HBG. On Onsager's Principle of Microscopic Reversibility. Rev Mod Phys. 1945;17:343-50.

[35] Mackay TG, Lakhtakia A. Electromagnetic anisotropy and bianisotropy: a field guide: World Scientific; 2009.

[36] Guo C, Zhao B, Fan S. Adjoint Kirchhoff's Law and General Symmetry Implications for All Thermal Emitters. Phys Rev X. 2022;12:021023.

[37] Li Z, Aydin K, Ozbay E. Determination of the effective constitutive parameters of bianisotropic metamaterials from reflection and transmission coefficients. Phys Rev E. 2009;79:026610.

[38] Han F-Y, Yin L-Z, Du C-H, Liu P-K. Robust Effective-Medium Characteristics of Bianisotropic Reflective Metasurfaces based on Field-Circuit Combined Analysis. Adv Theory Simul. 2021;4:2000246.

[39] Guo C, Fan S. Theoretical constraints on reciprocal and non-reciprocal many-body radiative heat transfer. Phys Rev B. 2020;102:085401.

[40] Liu T, Guo C, Li W, Fan S. Thermal photonics with broken symmetries. eLight. 2022;2:25.

[41] Teitler S, Henvis BW. Refraction in Stratified, Anisotropic Media. J Opt Soc Am. 1970;60:830-4.

[42] Berreman DW. Optics in stratified and anisotropic media: 4×4-matrix formulation. J Opt Soc Am. 1972;62:502-10.

[43] Khandekar C, Khosravi F, Li Z, Jacob Z. New spin-resolved thermal radiation laws for nonreciprocal bianisotropic media. New J Phys. 2020;22:123005.

[44] Álvarez-Pérez G, Folland TG, Errea I, Taboada-Gutiérrez J, Duan J, Martín-Sánchez J, et al. Infrared Permittivity of the Biaxial van der Waals Semiconductor α-MoO3 from Near- and Far-Field Correlative Studies. Adv Mater. 2020;32:1908176.

[45] Gabriel GJ, Brodwin ME. Distinctions Between Gyroelectric and Gyromagnetic Media in Rectangular Waveguide. IEEE Trans Microw Theory Tech. 1966;14:292-3.

[46] Zhao B, Shi Y, Wang J, Zhao Z, Zhao N, Fan S. Near-complete violation of Kirchhoff's law of thermal radiation with a 0.3 T magnetic field. Opt Lett. 2019;44:4203-6.

[47] Zhu L, Fan S. Near-complete violation of detailed balance in thermal radiation. Phys Rev B. 2014;90: 220301(R).

[48] Guo C, Asadchy VS, Zhao B, Fan S. Light control with Weyl semimetals. eLight. 2023;3:2.

[49] Maghrebi MF, Gorshkov AV, Sau JD. Fluctuation-Induced Torque on a Topological Insulator out of Thermal Equilibrium. Phys Rev Lett. 2019;123:055901.

[50] Talman R. Symmetry, physical laws, and electric dipole moments. The Electric Dipole Moment Challenge: Morgan & Claypool Publishers; 2017.

[51] Pyatakov AP, Zvezdin AK. Magnetoelectric and multiferroic media. Phys-Uspekhi. 2012;55:557.

[52] Smith DR, Gollub J, Mock JJ, Padilla WJ, Schurig D. Calculation and measurement of bianisotropy in a split ring resonator metamaterial. J Appl Phys. 2006;100:024507.

[53] Zhou J, Koschny T, Soukoulis CM. Magnetic and electric excitations in split ring resonators. Opt Express. 2007;15:17881-90.

[54] Zhao B, Guo C, Garcia CAC, Narang P, Fan S. Axion-field-enabled nonreciprocal thermal radiation in Weyl semimetals. Nano Lett. 2020;20:1923-7.